Application of Kalman Gain for Minimum Mean-Squared Phase-Error Bound in Bang-Bang CDRs

Joon-Yeong Lee and Hyeon-Min Bae, *Member, IEEE*

***Abstract*—This paper presents the minimum bound of the mean-squared phase-error of a bang-bang (BB) clock-and-data recovery (CDR) circuit under the condition of random phase tracking. An analogy between the Kalman filter and a linearized BB CDR is utilized for the derivation. The effects of demultiplexing, loop latency, and granular jitter are considered in the analysis to reflect reality. The validity of the theoretical analysis is supported by behavioral time domain simulation results.**

***Index Terms*—Bang-Bang PLL, Kalman filter, Markov process.**

I. Introduction

ANALOG domain CDRs implemented in nanometer CMOS technologies suffer from low voltage headroom, low output impedance of transistors, and large process variations [1]. Digital domain BB CDRs are being employed in serial links to overcome such challenges. Since the transfer function of a BB phase detector is nonlinear, the selection of design parameters and performance estimation have been performed empirically, based on behavioral time domain simulation results [2].

In this paper, we present the analytical minimum bounds of the mean squared phase error of a bang-bang (BB) clock-and-data recovery (CDR) circuit under the condition of random phase tracking. The analogy between the Kalman filter and a BB CDR is utilized for the derivation. The Kalman filter is a well-known optimal solution in tracking problems and the application of the Kalman filter to a PLL requires the acceptance of two assumptions: (i) the system is linear and (ii) the posterior mean squared error (MSE), defined as the phase difference between the desired and the output clock, at every time step is parameterized by the current MSE and the means and covariances of the non-accumulative period and accumulation jitter [3], [4]. The statistical quantities of such jitter can be estimated from the input signal with adaptive filtering techniques [5], [6]. The relationship between a linear PLL and the Kalman filter was initially discovered in [7], [8]. We have extended the previous works and applied the Kalman filter to a nonlinear BB CDR by linearizing the BBPD with the Markov chain method proposed in [9]. The optimal phase tracking performance of a BB CDR under various nonidealities, including loop latency and granular jitter, is estimated. The MSE is used to quantify the tracking performance of the BB CDR throughout the paper.

A phase rotator-based BB CDR was chosen for the analysis instead of a VCO-based counterpart since the phase rotator is digital-friendly and generally preferred in high speed parallel CDR designs [10]–[12]. Typically a phase rotator-based BB CDR has a first order loop because a frequency lock is achieved by a separate closed loop system as shown in Fig. 1. However, the proposed analysis can also be applied to any VCO-based type-2 designs because the second order loop is often over-damped, and hence behaves very similarly to a first-order loop [13].

Section II describes the linearization procedure and the estimated MSEs of a BB CDR with and without demultiplexing. Then, Section II-C presents the Kalman gain of a BB CDR and demonstrates the resulting minimum MSE bound. Section III offers in-depth analysis on the impact of implementation non-idealities such as control latency and the finite precision of the phase rotator to the minimum MSE bound. Finally, Section IV summarizes the discussion.

II. BB CDR and the Kalman Filter

Fig. 1 shows the Z-domain block diagram of a conventional rotator-based BB CDR. A clock generator provides frequency locked clocks to a digitally controlled phase rotator. Our analysis is restricted to the phase rotator loop shown in the shaded area. The CDR model consists of a BBPD, a loop filter with the gain and delay of β and D, respectively, and a digitally controlled phase rotator. The gain of a phase rotator θ_{pr} is related to its resolution, as given by

$$\theta_{pr} = \frac{1UI}{2^{RotatorResolution}}. \tag{1}$$

The input jitter of a CDR can be modeled as the sum of the accumulation and non-accumulative period jitter. The non-accumulative period jitter does not accumulate over time and has bounded variance in general. Data-dependent deterministic jitter is a subset of the non-accumulative jitter. The accumulation jitter, on the contrary, is unbounded in nature and increases indefinitely with time, thus a CDR has to track it for bit-error-free operation [7], [14], [15].

Manuscript received January 26, 2012; revised May 03, 2012; accepted May 24, 2012. This work was supported by the National Research Foundation of Korea (NRF) Grant funded by the Korea government (MEST) (No. 2011-0018356). Date of publication July 12, 2012; date of current version November 21, 2012. This paper was recommended by Associate Editor F. O'Mahony.

The authors are with the Department of Electrical Engineering, Korea Advanced Institute of Science and Technology (KAIST), Daejeon 305-701 Korea (e-mail: jy6218@kaist.ac.kr).

Digital Object Identifier 10.1109/TCSI.2012.2206460

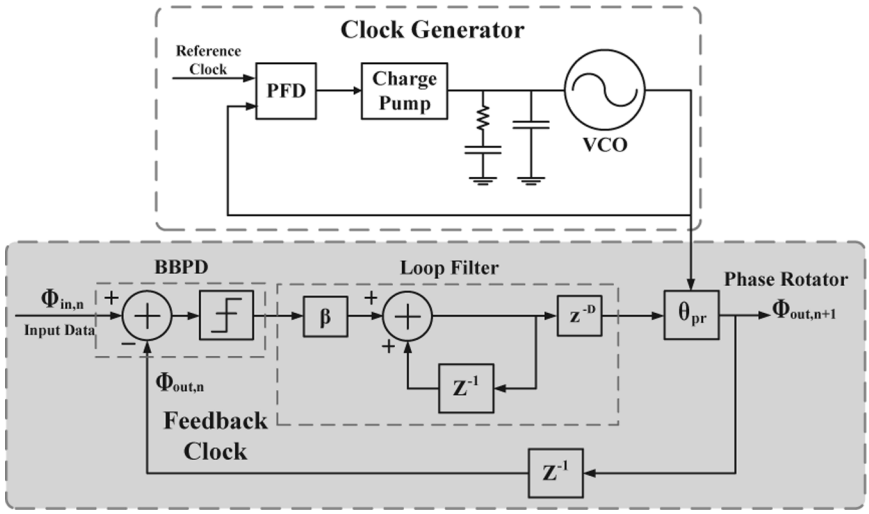

Fig. 1. Z-domain block diagram of a typical rotator-based BB CDR with a clock generator.

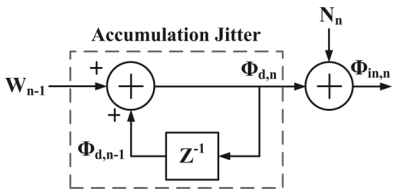

Fig. 2. Discrete time model of input jitter.

Fig. 2 shows the discrete time jitter model of a BB CDR. $\phi_{d,n}$ and N_n denote the accumulation and non-accumulative period jitter, respectively, at time index n. The accumulation jitter is modeled by a discrete time random walk process. By using the Z-transform, the power spectral density of the accumulation jitter is given by

$$S(f) = \frac{E[W^2]}{(1-z^{-1})(1-z)}\Big|_{z=e^{-j2\pi f/f_{Data}}} = \frac{E[W^2]}{4\sin^2(\frac{f\pi}{f_{Data}})} \quad (2)$$

where $E[W^2]$ is the variance of random period jitter W, and f_{Data} is the data rate. By taking the bilinear transformation of (2) for simplicity, we get

$$S(f) = \frac{E[W^2](1+(\frac{f\pi}{f_{Data}})^2)}{(\frac{2f\pi}{f_{Data}})^2}. \quad (3)$$

Note that $S(f)$ decreases by -20 dB/decade as frequency increases.

A jitter tolerance mask provides the information on the accumulation and random non-accumulative period jitter of a serial link. Fig. 3 shows a typical jitter tolerance mask [16]–[18]. The accumulation jitter dominates at low frequencies and decreases by -20 dB/decade as frequency increases. In a SONET jitter tolerance mask, the magnitude of random non-accumulative period jitter intersects with the accumulation jitter at $1/2500$th of the data rate [16].

The magnitude of $S(f)$ can be estimated with the jitter tolerance mask since it represents the maximum permissible jitter

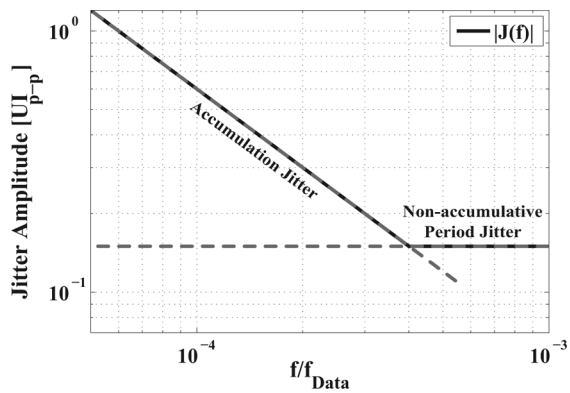

Fig. 3. Typical shape of jitter tolerance mask.

present in a communication link. Even if the practical jitter in a link is hardly composed of sinusoids, the jitter tolerance specification is defined with sinusoids for testing purposes. In practice, the jitter in serial links carrying real traffic is more like random noise [16].

Appropriate values for σ_W and σ_N can be estimated by matching the variances of the modeled jitter in Fig. 2 with that of a sinusoid defined in the jitter tolerance mask. Let the magnitude of the jitter tolerance mask be $J(f)$, and W and N are white Gaussian processes. $|S(f)|$ should then satisfy $|S(f)| = |J(f)|^2/8$. For a SONET jitter mask, σ_W and σ_N are $(0.6\pi/\sqrt{2}) \times 10^{-4} UI_{rms}$ and $0.053 UI_{rms}$, respectively, and note that $\sigma_N \gg \sigma_W$.

A. Phase Domain MSE of a BB CDR

Fig. 4 shows the phase-domain discrete-time block diagram of a linearized BB CDR including input jitter. A nonlinear BBPD is linearized by using a Markov chain analogy in phase lock [9]. The linearized BBPD consists of linear gain K_{bbpd} with quantization noise ϕ_{bbpd}. The equivalent gain K_{bbpd} is given by

$$K_{bbpd} = \frac{1}{\sqrt{2\pi}\sigma_J}[1 + e^{-(1/2)(\beta\theta_{pr}/\sigma_J)^2}] \quad (4)$$

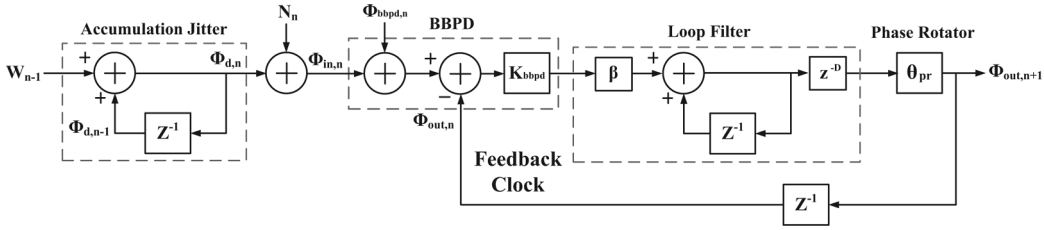

Fig. 4. Phase-domain discrete-time model of a linearized BB CDR and input jitter.

where σ_J is the standard deviation of the relative input Gaussian jitter $\phi_J = \phi_{\rm in} - \phi_{\rm out}$. According to [19], ϕ_{bbpd} can be modeled by a white random process uncorrelated with ϕ_J if $\sigma_J \gg \beta\theta_{pr}$. The standard deviation of ϕ_{bbpd} is approximately $0.75\sigma_J$. In case $\sigma_J \leq 0.5\beta\theta_{pr}$, the dynamics of a BB CDR are merely nonlinear, and hence, this case is not considered in this paper.

Let the n-th prediction error, e_n, be

$$e_n = \phi_{d,n} - \phi_{out,n} \tag{5}$$

where $\phi_{d,n}$ and $\phi_{out,n}$ are the n-th desired and the output clock phases, respectively. If we neglect computational latency D, for simplicity, the $n+1$-th prediction error, e_{n+1}, is recursively given by

$$\begin{aligned} e_{n+1} &= \phi_{d,n+1} - \phi_{out,n+1} \\ &= (1 - K_{bbpd}\beta\theta_{pr})e_n + W_n \\ &\quad - K_{bbpd}\beta\theta_{pr}(N_n + \phi_{bbpd,n}). \end{aligned} \tag{6}$$

The MSE of the $n+1$-th prediction error is

$$\begin{aligned} E[e_{n+1}^2] = (1 - K_{bbpd}\beta\theta_{pr})^2 E[e_n^2] + E[W_n^2] \\ + K_{bbpd}^2\beta^2\theta_{pr}^2(E[N_n^2] + \frac{9}{16}\sigma_J^2) \end{aligned} \tag{7}$$

where $E[\phi_{bbpd,n}^2] \approx 9\sigma_J^2/16$ under phase lock [19]. Provided that the CDR bandwidth is sufficiently large to track the accumulation jitter, σ_J^2 is approximately $E[W^2]+E[N^2]$. By setting $E[e_{n+1}^2] = E[e_n^2] = E[e_\infty^2]$, the steady state MSE is given by

$$E[e_\infty^2] = \frac{(1+\frac{9}{16}K_{bbpd}^2\beta^2\theta_{pr}^2)E[W^2]+\frac{25}{16}K_{bbpd}^2\beta^2\theta_{pr}^2E[N^2]}{2K_{bbpd}\beta\theta_{pr} - K_{bbpd}^2\beta^2\theta_{pr}^2} \tag{8}$$

where $E[W_n^2] = E[W^2]$ and $E[N_n^2] = E[N^2]$. In case $E[W^2] = 0$, by using (4), (8) is simplified to $E[e_\infty^2] \approx 25/(16\sqrt{2\pi})\theta_{pr}\beta\sigma_N$, which coincides with the previous result presented in [19].

Fig. 5 shows the analytical and simulated MSEs of a BB CDR with $\sigma_W = (0.6\pi/\sqrt{2}) \times 10^{-4}UI_{rms}$. The gain of the loop filter is set $\beta = 1$. The behavioral simulation results validate the theoretical analysis in the meaningful σ_N range.

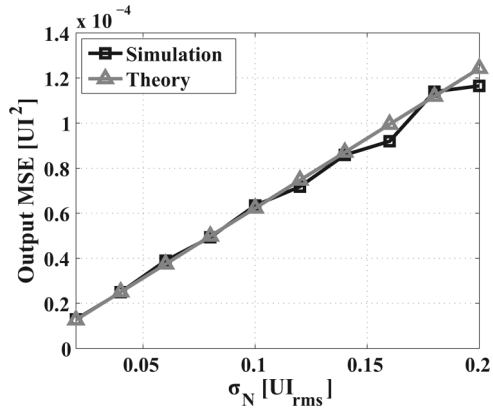

Fig. 5. Output MSE of the single BB CDR with $\sigma_W = (0.6\pi/\sqrt{2}) \times 10^{-4}UI_{rms}$.

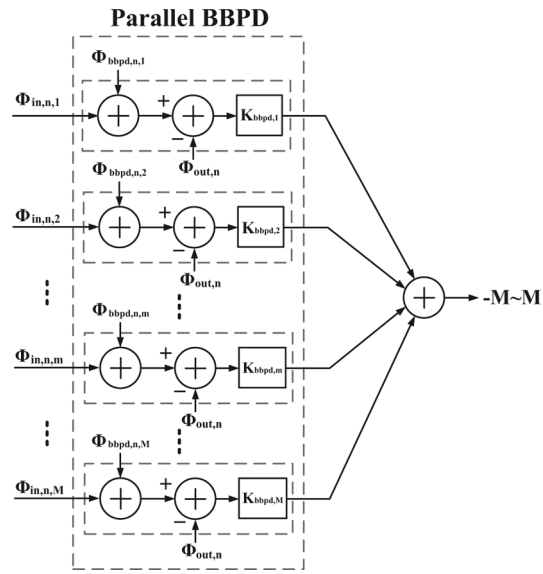

Fig. 6. Linearized discrete-time block diagram of a $1:M$ demultiplexed parallel BBPD.

B. MSE Under Demultiplexed Phase Update

High-speed digital domain CDRs typically make parallel demultiplexed subrate phase updates due to timing constraints of digital logic blocks. Fig. 6 shows the linearized discrete time block diagram of a $1:M$ demultiplexed BBPD. A demultiplexer is modeled by parallel BBPDs with a subsequent summation block.

Let $e_{n,m}$ be the n-th prediction error of the m-th channel in the set of parallel BBPDs as given by $e_{n,m} = \phi_{d,n,m} - \phi_{out,n,m}$. The time and channel indexes satisfy $-\infty < n < \infty$ and $0 < m \leq M$, respectively, where M is the level of parallelization. The linearized gain of the m-th BBPD, $K_{bbpd,m}$, is $2/\sqrt{2\pi(m\sigma_W^2 + \sigma_N^2)}$, since the random jitter W is accumulated for m cycles. In the case of $\sigma_W \ll \sigma_N$, this linearized gain becomes insensitive to the channel index m and can be approximated as $K_{bbpd,m} \approx 2/(\sqrt{2\pi}\sigma_N) = K_{bbpd}$.

A recursive equation for the $n+1$-th prediction error of the first channel, $e_{n+1,1}$, is given by

$$e_{n+1,1} = e_{n,M} + W_{n,1} - (Me_{n,1} + \sum_{k=2}^{M}(M+1-k)W_{n-1,k} + \sum_{k=1}^{M}(N_{n,k} + \phi_{bbpd,n,k}))K_{bbpd}\beta\theta_{pr}. \quad (9)$$

$e_{n,m}$ is related to $e_{n,1}$ by

$$e_{n,m} = e_{n,1} + \sum_{k=2}^{m} W_{n-1,k} \quad (10)$$

since the phase updates occur every M-th input signal. By substituting (10) into (9), we get

$$e_{n+1,1} = e_{n,1} + \sum_{k=2}^{M} W_{n-1,k} + W_{n,1} - (Me_{n,1} + \sum_{k=2}^{M}(M+1-k)W_{n-1,k} + \sum_{k=1}^{M}(N_{n,k} + \phi_{bbpd,n,k}))K_{bbpd}\beta\theta_{pr}. \quad (11)$$

The MSE of the first channel is given by

$$E[e_{n+1,1}^2] = (1 - MK_{bbpd}\beta\theta_{pr})^2 E[e_{n,1}^2] + \sum_{k=1}^{M-1}(1-(M-k)K_{bbpd}\beta\theta_{pr})^2 E[W_{n-1,k+1}^2] + \frac{9}{16}\frac{M(M+1)(2M+1)}{6}\beta^2 K_{bbpd}^2\theta_{pr}^2 E[W^2] + E[W^2] + \frac{25}{16}M\beta^2 K_{bbpd}^2\theta_{pr}^2 E[N^2] \quad (12)$$

where $E[(\sum_{k=1}^{M}\phi_{bbpd,n,k})^2] = (9/16)\sum_{k=1}^{M}(\sigma_N^2 + k^2\sigma_W^2)$ under phase lock [19]. By defining the MSE at $n+1$-th clock cycle as the average MSE among M parallel channels, we get

$$E[e_{n+1}^2] = \frac{\sum_{k=1}^{M} E[e_{n+1,k}^2]}{M} = E[e_{n+1,1}^2] + \frac{M-1}{2}E[W^2]. \quad (13)$$

By substituting (12) into (13), we get

$$E[e_{n+1}^2] = (1 - MK_{bbpd}\beta\theta_{pr})^2 E[e_n^2] + (M + (\frac{9}{16}\frac{M(M+1)(2M+1)}{6} - \frac{M(M-1)(M+1)}{6})\beta^2 K_{bbpd}^2\theta_{pr}^2)E[W^2] + \frac{25}{16}M\beta^2 K_{bbpd}^2\theta_{pr}^2 E[N^2] \quad (14)$$

where $E[W_{n-1,k}^2] = E[W_{n,k}^2] = E[W^2]$ and $E[N_{n-1,k}^2] = E[N_{n,k}^2] = E[N^2]$. The steady state MSE is given by

$$E[e_\infty^2] = \frac{ME[W^2] + M\beta^2 K_{bbpd}^2\theta_{pr}^2\eta}{2MK_{bbpd}\beta\theta_{pr} - M^2 K_{bbpd}^2\beta^2\theta_{pr}^2} \quad (15)$$

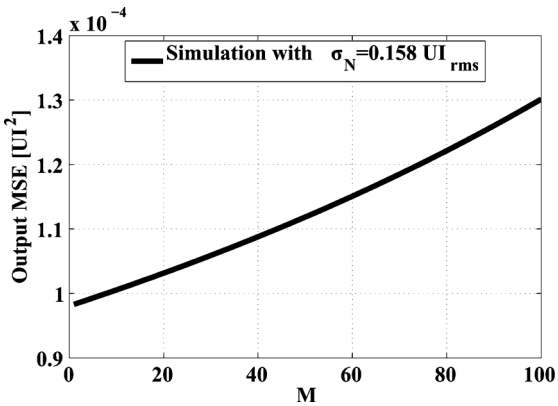

Fig. 7. Output MSE of the demuxed BB CDR versus M, with $\sigma_W = (0.6\pi/\sqrt{2}) \times 10^{-4}UI_{rms}$ and $\sigma_N = 0.158UI_{rms}$.

where $\eta = \lambda E[W_n^2] + (25/16)E[N_n^2]$ and $\lambda = (9/16)((M+1)(2M+1)/6) - ((M-1)(M+1)/6)$.

Fig. 7 shows the simulation result of the MSE with respect to M when $\sigma_W = (0.6\pi/\sqrt{2}) \times 10^{-4}UI_{rms}$ and $\sigma_N = 0.158UI_{rms}$. The MSE increases in proportion to M since the phase update latency degrades the tracking performance.

C. Minimum MSE Bound With Kalman Gain

The Kalman filter is a discrete time minimum MSE estimator that finds the optimum Kalman gain by minimizing the posterior MSE recursively. The tracking error in a BB CDR can be minimized by incorporating the Kalman filter algorithm in selecting the optimum forward gain β. The optimum Kalman gain achieves the optimum balance between tracking the accumulation jitter and filtering the non-accumulative period jitter.

Let B_n be β at time index n. By taking the derivative of $E[e_{n+1}^2]$ in (14) with respect to B_n, we get

$$\frac{dE[e_{n+1}^2]}{dB_n} = -2(1 - MK_{bbpd}B_n\theta_{pr})MK_{bbpd}\theta_{pr}E[e_n^2] + (\frac{9}{16}\frac{M(M+1)(2M+1)}{3} - \frac{M(M-1)(M+1)}{3})B_nK_{bbpd}^2\theta_{pr}^2E[W^2] + \frac{25}{8}MB_nK_{bbpd}^2\theta_{pr}^2E[N^2]. \quad (16)$$

Optimum Kalman gain B_n satisfying $dE[e_{n+1}^2]/dB_n = 0$ is

$$B_n = \frac{1}{K_{bbpd}\theta_{pr}}\frac{E[e_n^2]}{ME[e_n^2] + \lambda E[W_n^2] + \frac{25}{16}E[N_n^2]}. \quad (17)$$

By substituting (17) into (14) for simplicity, we get

$$E[e_{n+1}^2] = (1 - MB_nK_{bbpd}\theta pr)E[e_n^2] + ME[W_n^2]. \quad (18)$$

Equation (17) and (18) yield the recursive procedure that constitutes the Kalman filtering algorithm. The steady state MSE is

$$E[e_\infty^2] = \frac{ME[W^2] + \sqrt{M^2E[W^2]^2 + 4\eta E[W^2]}}{2} \quad (19)$$

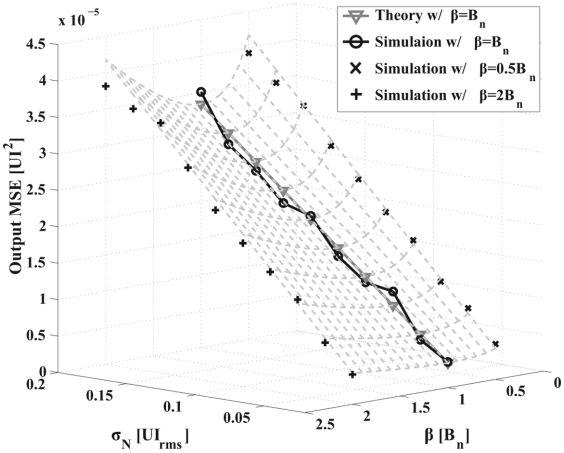

Fig. 8. Analytical and simulated MSEs of a 1:8 demultiplexed BB CDR under various gains with $\sigma_W = (0.6\pi/\sqrt{2}) \times 10^{-4} UI_{rms}$, and $D = 0$.

where $E[W_n^2] = E[W^2]$ and $E[N_n^2] = E[N^2]$. Equation (19) indicates the minimum MSE bound of a BB CDR.

Fig. 8 shows the analytical and simulated MSEs of a 1:8 demultiplexed BB CDR with Kalman gain. The theoretical and simulated results show close agreement, and the MSEs are minimized when the Kalman gains are applied.

III. MSE Under Implementation Nonidealities

In the previous section, implementation nonidealities such as latency in the loop filter and quantization noise from the phase rotator are neglected for simplicity in the analysis. Control latency, however, degrades the tracking performance of a CDR by decreasing the closed loop phase margin [20]. Digitally controlled phase rotators have limited resolution for the output phase. Reduced resolution relaxes the complexity of a rotator [10]–[12] while degrading the jitter performance of a CDR [21].

A. Latency in the Loop Filter

In case delay in the loop filter D is nonzero, (11) is modified as

$$\begin{aligned} e_{n+1,1} = e_{n,1} &+ \sum_{k=2}^{M} W_{n-1,k} + W_{n,1} \\ &- (Me_{n-D,1} + \sum_{k=2}^{M}(M+1-k)W_{n-D-1,k} \\ &+ \sum_{k=1}^{M}(N_{n-D,k} + \phi_{bbpd,n-D,k}))K_{bbpd}B_n\theta_{pr}. \end{aligned} \quad (20)$$

According to [20], K_{bbpd} can be approximated as $K_{bbpd} = 2q_0/(\sqrt{2\pi}\sigma_J)$ if $\sigma_J < B_n/K_{bbpd}$, where q_0 is $1/2$, $1/3$, and $1/5$ for $D = 0$, 1 and 2, respectively. However, in the case of $\sigma_J > B_n/K_{bbpd}$, which is the main focus of this paper, $K_{bbpd} = 2/(\sqrt{2\pi}\sigma_J)$ and is independent of the loop delay.

In order to calculate the MSE under nonzero loop delay, the correlation between $e_{n,1}$ and $e_{n-D,1}$ should be considered.

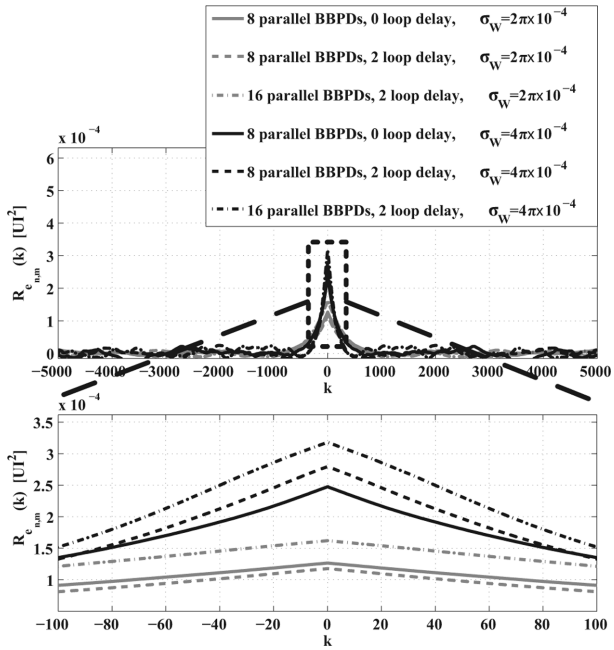

Fig. 9. Simulated autocorrelation of $e_{n,m}$ with $\sigma_N = 0.158 UI_{rms}$.

Fig. 9 shows the simulated autocorrelation of $e_{n,m}$ for various levels of parallelization, loop delays, and input accumulation jitters when gain B_n, defined in (17), is used. The autocorrelation $R_{e_{n,m}}(k)$ is given by $E[err(Mn+m)err(Mn+m+k)]$, where $err(Mn+m) = e_{n,m}$. It clearly demonstrates that $e_{n,m}$ can be approximated as a white process except in the vicinity of the origin. Small $E[e_{n,1}e_{n-D,1}]$ makes B_n remain close to the optimum value under nonzero loop delay.

Close examination of Fig. 9 reveals that the slope of the autocorrelation near the origin is close to $E[W^2]$, irrespective of D and M. By using this observation result, the expectation value of $e_{n,1}e_{n-D,1}$ can be approximated as

$$E[e_{n,1}e_{n-D,1}] \approx E[e_{n,1}^2] - MDE[W_n^2]. \quad (21)$$

By using (21), $E[(e_{n,1} - MB_{Dn}K_{bbpd}\theta_{pr}e_{n-D,1})^2]$ becomes

$$\begin{aligned} &E[(e_{n,1} - MB_{Dn}K_{bbpd}\theta_{pr}e_{n-D,1})^2] \\ &\quad = (1 - MB_{Dn}K_{bbpd}\theta_{pr})^2 E[e_{n,1}^2] \\ &\qquad + 2M^2 DB_{Dn}K_{bbpd}\theta_{pr}E[W_n^2]. \end{aligned} \quad (22)$$

From (20) and (22), the recursive MSE equation with nonzero D is

$$\begin{aligned} E[e_{n+1}^2] &= (1 - MK_{bbpd}B_{Dn}\theta_{pr})^2 E[e_n^2] \\ &\quad + (M + (\frac{9}{16}\frac{M(M+1)(2M+1)}{6} \\ &\qquad - \frac{M(M-1)(M+1)}{6})B_{Dn}^2 K_{bbpd}^2 \theta_{pr}^2)E[W^2] \\ &\quad + \frac{25}{16}MB_{Dn}^2 K_{bbpd}^2 \theta_{pr}^2 E[N^2] \\ &\quad + 2M^2 DB_{Dn}K_{bbpd}\theta_{pr}E[W^2] \end{aligned} \quad (23)$$

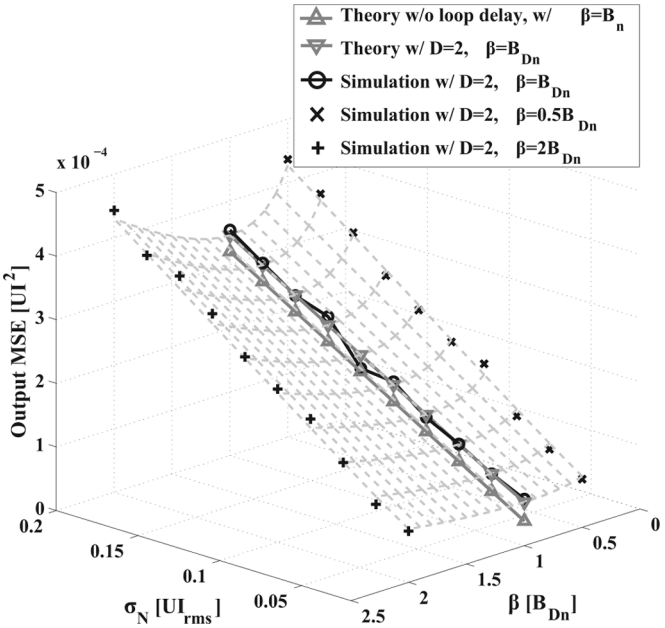

Fig. 10. Analytical and simulated MSEs of a 1:8 demultiplexed BB CDR with Kalman gain with $\sigma_W = 4\pi \times 10^{-4} UI_{rms}$, $D = 2$.

where B_{Dn} denotes the Kalman gain with loop delay. By taking a similar approach to (16), Kalman gain B_{Dn} is

$$B_{Dn} = \frac{1}{K_{bbpd}\theta_{pr}} \frac{E[e_n^2] - MDE[W_n^2]}{ME[e_n^2] + \lambda E[W_n^2] + \frac{25}{16}E[N_n^2]}. \quad (24)$$

The Kalman gain under control latency is smaller than (17), because only low frequency prediction error is valid. By the way, in most cases, the tracking error satisfies $E[e_n^2] \gg E[W^2]$ in the locked condition, than $B_{Dn} \approx B_n$. By substituting (24) into (23), we get

$$E[e_{n+1}^2] = (1 - MB_{Dn}K_{bbpd}\theta_{pr})E[e_n^2] + (M + M^2DB_{Dn}K_{bbpd}\theta_{pr})E[W_n^2] \quad (25)$$

and the steady state MSE is

$$E[e_\infty^2] = \frac{(2D+1)ME[W^2]}{2} + \frac{\sqrt{M^2(4D+1)E[W^2]^2 + 4\eta E[W^2]}}{2} \quad (26)$$

where $E[W_n^2] = E[W^2]$ and $E[N_n^2] = E[N^2]$. Equation (26) represents the generalized minimum MSE bound of a BB CDR. This bound is equal to (19), when $D = 0$.

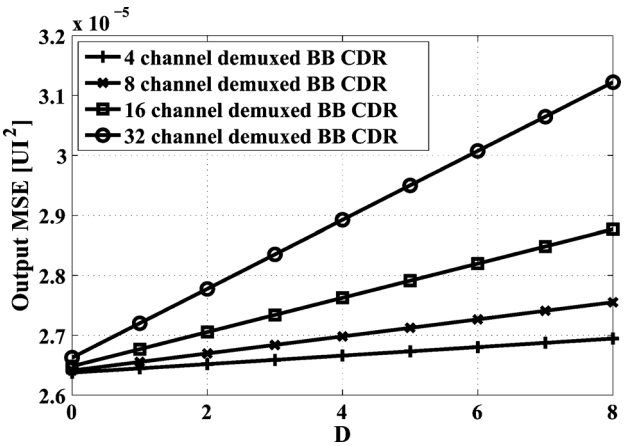

Fig. 11. MSE versus loop delay D ($\sigma_W = (0.6\pi/\sqrt{2}) \times 10^{-4} UI_{rms}, \sigma_N = 0.158 UI_{rms}$).

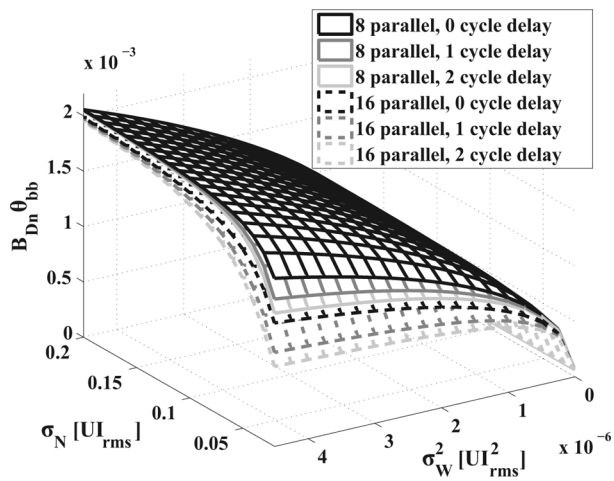

Fig. 12. $B_{Dn}\theta_{pr}$ versus σ_N and σ_W^2.

Fig. 10 shows the analytical and simulated MSEs with various loop gains. The analytical results match strongly with the simulated results, and it is clear that the MSE is at a minimum when the optimum gain B_{Dn} is employed.

Fig. 11 shows the relationship between the minimum MSE bound and loop delay D under various demultiplexing ratios when $\sigma_W = (0.6\pi/\sqrt{2}) \times 10^{-4} UI_{rms}$ and $\sigma_N = 0.158 UI_{rms}$. The minimum MSE bound increases in proportion to D and M.

Fig. 12 shows the optimum value of $B_{Dn}\theta_{pr}$ for the minimum MSE with respect to σ_N and σ_W^2 in steady state. $B_{Dn}\theta_{pr}$ is inversely proportional to D and M and proportional to the variances of the non-accumulative period and accumulation jitter.

By substituting (26) into (24), the optimum forward gain $B_{Dn}\theta_{pr}$ is given by see equation (27) at the bottom of the page.

$$B_{Dn}\theta_{pr} = \frac{\sqrt{2\pi}\sigma_N}{2} \frac{\left(M\sigma_W^2 + \sqrt{M^2(4D+1)\sigma_W^4 + 4\eta\sigma_W^2}\right)}{\left((2D+1)M^2\sigma_W^2 + M\sqrt{M^2(4D+1)\sigma_W^4 + 4\eta\sigma_W^2} + 2\lambda\sigma_W^2 + \frac{25}{8}\sigma_N^2\right)} \quad (27)$$

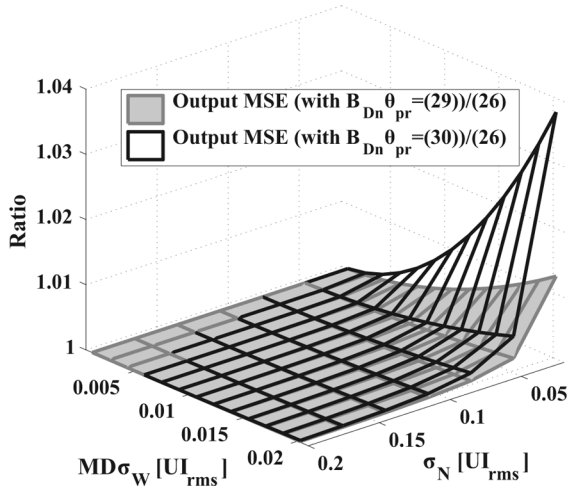

Fig. 13. Ratio between the output MSEs simulated with (29), (30) and optimum gain $B_{Dn}\theta_{pr}$ versus $MD\sigma_W$ and σ_N.

In the case of $\sigma_W \ll \sigma_N$, $\sqrt{M^2(4D+1)\sigma_W^4 + 4\eta\sigma_W^2} \approx (5/2)\sigma_W\sigma_N$, and hence, (27) can be simplified to

$$B_{Dn}\theta_{pr} \approx \frac{M\sigma_W^2 + \frac{5}{2}\sigma_W\sigma_N}{2M\sigma_W + \frac{5}{2}\sigma_N} \tag{28}$$

By using a Taylor series, (28) can be further simplified as given by

$$B_{Dn}\theta_{pr} \approx (1 - \frac{2M\sigma_W}{5\sigma_N})\sigma_W \tag{29}$$

$$\approx \sigma_W. \tag{30}$$

Because a PLL is designed to track the accumulation jitter, the forward gain, which represents the bandwidth of a PLL, should be mainly related to the accumulation jitter; the optimum bandwidth is approximately the standard deviation of the step size of the accumulation jitter.

Fig. 13 shows the ratio between the output MSEs simulated with (29), (30), and optimum $B_{Dn}\theta_{pr}$. The MSE using (29) is greater than the minimum bound by 1% for $\sigma_N > 0.02UI_{rms}$ and $MD\sigma_W < 0.02UI_{rms}$. The MSE using (30) deviates even further from the minimum bound but the difference is still less than 4% for $\sigma_N > 0.02UI_{rms}$ and $MD\sigma_W < 0.02UI_{rms}$.

B. Limited Phase Rotator Resolution

The quantization noise of the phase rotator is inversely proportional to its resolution and degrades the MSE. Fig. 14 shows the simulated MSE of a BB CDR with $M = 8$ and $D = 0$ versus the input non-accumulative period jitter under various phase rotator resolutions. Kalman gains are adjusted to achieve $B_{Dn}\theta_{pr} \approx \sigma_W$. The MSE is dominated by the quantization noise if the resolution of the phase rotator is less than 7 bits. The degradation of the MSE caused by non-accumulative period jitter is negligible in this case.

Fig. 15 shows the simulated probability mass function (PMF) of the prediction error $(e = \phi_d - \phi_{\text{out}})$ under various resolutions of the phase rotator. Small non-accumulative period jitter

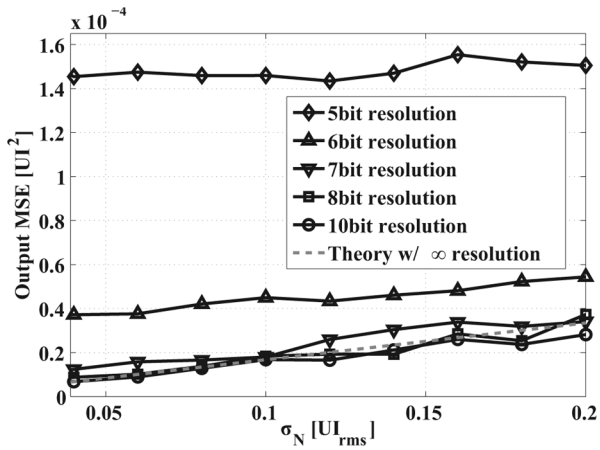

Fig. 14. MSEs of the 1:8 demultiplexed BB CDR with Kalman gain under various phase rotator resolutions ($\sigma_W = (0.6\pi/\sqrt{2}) \times 10^{-4} UI_{rms}, D = 0$).

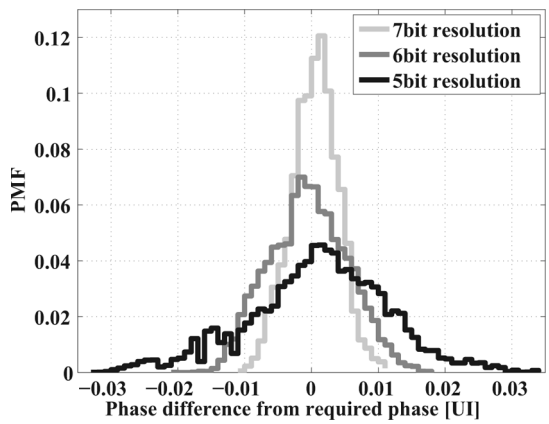

Fig. 15. Simulated PMF of the prediction error under various phase rotator resolutions with $\sigma_N = 0.05UI_{rms}$, $\sigma_W = (0.6\pi/\sqrt{2}) \times 10^{-4} UI_{rms}$, and $D = 0$.

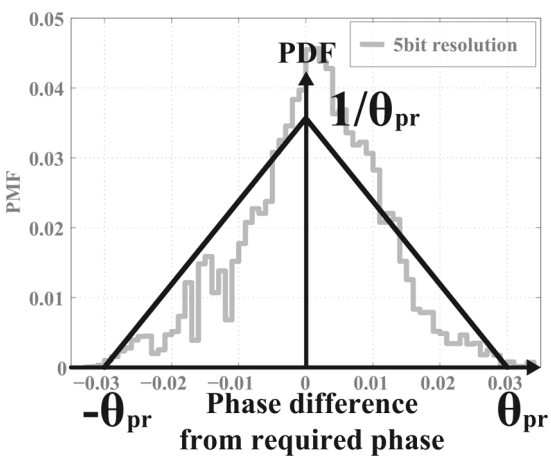

Fig. 16. Modeling of the PMF with a triangular PDF.

of $\sigma_N = 0.05UI_{rms}$ is chosen to highlight the quantization effect. The shape of the PMF broadens as the resolution decreases. The PMF of the output prediction error can be modeled by a triangular probability density function (PDF), as shown in Fig. 16.

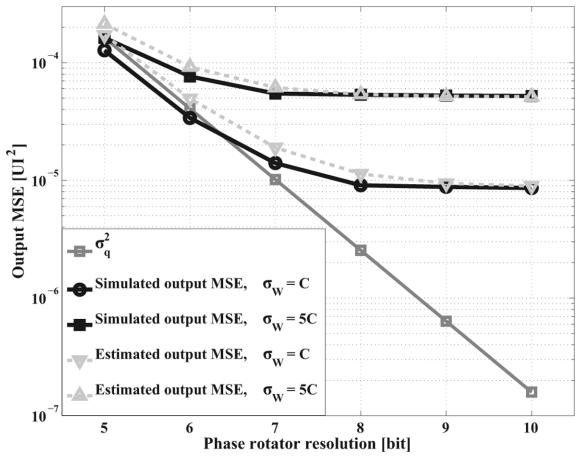

Fig. 17. σ_q^2 and the simulated and estimated output MSE of 1:8 demultiplexed BB CDR with Kalman gain versus various phase rotator resolutions with $\sigma_N = 0.05UI_{rms}$, $C = (0.6\pi/\sqrt{2}) \times 10^{-4}UI_{rms}$, and $D = 2$.

The analytical variance of the prediction error calculated with the triangular model is

$$\sigma_q^2 = 2\int_0^{\theta_{pr}} e^2\left(\frac{1}{\theta_{pr}} - \frac{e}{\theta_{pr}^2}\right)de = \frac{\theta_{pr}^2}{6}. \tag{31}$$

Our model overestimates the variance by 6.67%. The variance of the prediction error is equal to the output MSE since the prediction error is unbiased and has zero mean [22].

Total output MSE considering both nonzero loop delay and the quantization noise of the phase rotator can be approximated, by using (26) and (31), as

$$MSE \approx \frac{\theta_{pr}^2}{6} + \frac{(2D+1)ME[W^2]}{2} + \frac{\sqrt{M^2(4D+1)E[W^2]^2 + 4\eta E[W^2]}}{2}. \tag{32}$$

Fig. 17 shows σ_q^2 and the simulated and estimated output MSE under various resolutions of the phase rotator at $\sigma_N = 0.05UI_{rms}$. The simulated MSE converges asymptotically to σ_q^2 at low resolutions since the quantization noise dominates the output MSE. The resolution of the phase rotator should be set to greater than 7 bits to make the quantization effect negligible when $\sigma_W = (0.6\pi/\sqrt{2}) \times 10^{-4}UI_{rms}$.

IV. Summary

The optimum forward gain and the resulting minimum phase error bounds of a BB CDR are presented. The optimum gain is approximately σ_W. Provided that σ_W is estimated in real time, a BB CDR can adaptively accomplish the optimum balance between tracking and filtering the input jitter. The resolution of the phase rotator should be set greater than 5 bits to suppress the output jitter to below $0.02UI_{rms}$ under practical input jitter conditions.

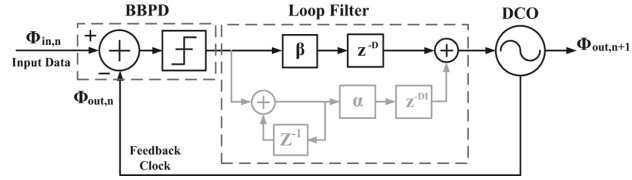

Fig. 18. Block diagram of VCO-based type-2 digital BB CDR.

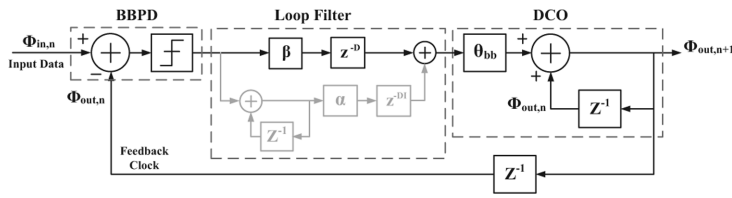

Fig. 19. Z-domain block diagram of a VCO-based type-2 digital BB CDR.

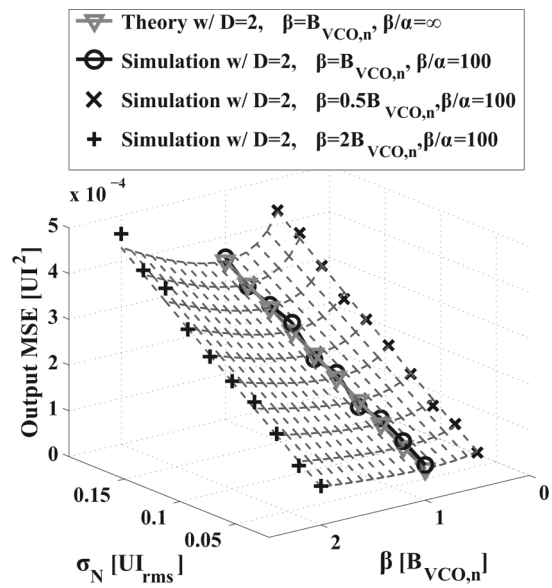

Fig. 20. The analytical and simulated MSEs of a 1:8 demultiplexed VCO-based BB CDR with Kalman gain with $\beta/\alpha = 100$, $\sigma_W = 4\pi \times 10^{-4}UI_{rms}$, $D = DI = 2$.

Appendix
Minimum MSE Bound of a VCO-Based Type-2 BB CDR

Fig. 18 shows the block diagram of a conventional type-2 VCO-based digital BB CDR. The proportional and integral path gains are β and α, respectively, and DI denotes the integral path delay. The proportional gain should be greater than the integral step gain to ensure stable operation [1].

Fig. 19 shows the Z-domain block diagram of a highly overdamped VCO-based type-2 digital BB CDR [2]. The phase step of the loop is given by

$$\theta_{bb} = \frac{K_{VCO}}{f_0}[UI] \tag{33}$$

where K_{VCO} and f_0 denote the VCO gain and nominal frequency, respectively. In the case of $\alpha = 0$, the only difference between the phase rotator-based and VCO-based BB CDR is the location of a phase accumulator. Therefore, (24) can also be applied to a VCO-based design by replacing θ_{pr} with θ_{bb}.

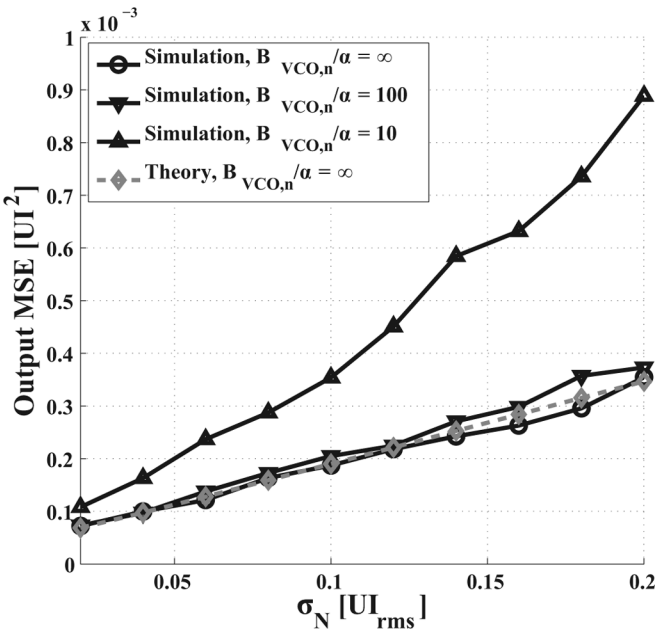

Fig. 21. Analytical and simulated MSEs of a 1:8 demultiplexed VCO-based BB CDR with Kalman gain with $\sigma_W = 4\pi \times 10^{-4} UI_{rms}$, $D = DI = 2$.

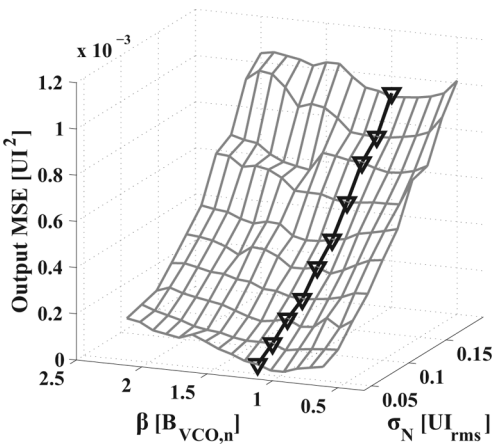

Fig. 22. Simulated MSE of a 1:8 demultiplexed VCO-based BB CDR with Kalman gain with $\beta/\alpha = 10$, $\sigma_W = 4\pi \times 10^{-4} UI_{rms}$, $D = DI = 2$.

Fig. 20 shows the analytical and simulated MSEs with the Kalman gain, when the loop is highly over-damped ($\beta/\alpha \geq 100$). The analytical results match strongly with the simulated results, and it is clear that the MSE is at a minimum when the Kalman gain $B_{VCO,n}$ is employed.

The MSE is inversely proportional to β/α, owing to an oscillatory overshoot [13], and hence the minimum MSE can be achieved by designing a highly over-damped BB CDRs. Fig. 21 shows the analytical and simulated MSEs with various stability factors when $B_{VCO,n}$ is employed. The MSE is degraded as β/α decreases. By the way, we have noticed through simulation that the MSE has a local minimum around $\beta \approx B_{VCO,n}$ even in a system with a low damping and Fig. 22 validates our observations.

REFERENCES

[1] H. S. Song, D. S. Kim, D. H. Oh, S. H. Kim, and D. K. Jeong, "A 1.0–4.0-Gb/s all-digital CDR with 1.0-ps period resolution DCO and adaptive proportional gain control," *IEEE J. Solid-State Circuits*, vol. 46, no. 2, pp. 424–434, Feb. 2011.

[2] S. Tertinek, J. P. Gleeson, and O. Feely, "Statistical analysis of first-order bang-bang phase-locked loops using sign-dependent random-walk theory," *IEEE Trans. Circuits Syst. I, Reg. Papers.*, vol. 57, no. 9, pp. 2367–2380, Sep. 2010.

[3] A. L. Garcia, *Probability and Random Processes for Electrical Engineering*, 2nd ed. New York: Addison-Wesley, 1994, pp. 439–443.

[4] F. M. Gardner, *Phaselock Techniques*, 3rd ed. Hoboken, NJ: Wiley, 2005.

[5] B. M. Akesson, J. B. Jorgensen, and S. B. Jorgensen, "A generalized autocovariance least-squares method for covariance estimation," in *IEEE Amer. Control Conf.*, Jul. 2007, pp. 3713–3714.

[6] M. F. Abdel-Hafez, "The autocovariance least-squares technique for GPS measurement noise estimation," *IEEE Trans. Vehicular Tech.*, vol. 59, no. 2, pp. 574–588, Feb. 2010.

[7] P. F. Driessen, "DPLL bit synchronizer with rapid acquisition using adaptive kalman filtering techniques," *IEEE Trans. Commun.*, vol. 42, no. 9, pp. 2673–2675, Sep. 1994.

[8] G. S. Christiansen, "Modeling of PRML timing loop as a Kalman filter," in *IEEE Int. Global Telecommunications Conf.*, 1994, pp. 1157–1161.

[9] N. D. Dalt, "Markov chains-based derivation of the phase detector gain in bang-bang PLLs," *IEEE Trans. Circuits Syst. II, Exp Briefs.*, vol. 53, no. 11, pp. 1195–1199, Nov. 2006.

[10] M. Fukaishi, K. Nakamura, H. Heiuchi, Y. Hirota, Y. Nakazawa, H. Ikeno, H. Hayama, and M. Yotsuyanagi, "A 20 Gb/s CMOS multichannel transmitter and receiver chip set for ultrahigh resolution digital display," in *IEEE Int. Solid-State Circuits Conf. Dig. Tech. Papers*, Feb. 2000, vol. 463, pp. 260–261.

[11] H. Takauchi, H. Tamura, S. Matsubara, M. Kibune, Y. Doi, T. Chiba, H. Anbutsu, H. Yamaguchi, T. Mori, M. Takatsu, K. Gotoh, T. Sakai, and T. Yamamura, "A CMOS multichannel 10-Gb/s transceiver," *IEEE J. Solid-State Circuits*, vol. 38, no. 12, pp. 2094–2100, Dec. 2003.

[12] H. Wang and A. Hajimiri, "A wideband CMOS linear digital phase rotator," in *IEEE Int. Custom Integr. Circuits Conf.*, 2007, pp. 671–674.

[13] B. Razavi, *Phase-Locking in High-Performance Systems: From Devices to Architectures*, 1st ed. Hoboken, NJ: Wiley-IEEE Press, 2005, pp. 34–45.

[14] B. Razavi, "Challenges in the design high-speed clock and data recovery circuits," *IEEE Commun. Mag.*, vol. 40, no. 8, pp. 94–101, Aug. 2002.

[15] V. Stojanovic and M. Horowitz, "Modeling and analysis of high-speed links," in *Proc. IEEE Int. Custom Integr. Circuits Conf.*, 2003, pp. 589–594.

[16] *"Understanding Jitter and Wander Measurements and Standards,"* 2nd ed. Agilient Technologies UK LTD, 2003.

[17] *"VESA DisplayPort Standard,"* Video Electronics Standards Association, 2010, pp. 341–352.

[18] *"Universal Serial Bus 3.0 Specification,"* Hewlett-Packard Company, Intel, Microsoft, NEC Corporation, ST-NXP Wireless, and Texas Instruments, 2008.

[19] N. D. Dalt, "Linearized analysis of a digital bang-bang PLL and its validitiy limits applied to jitter transfer and jitter generation," *IEEE Trans. Circuits Syst. I, Reg. Papers.*, vol. 55, no. 11, pp. 3663–3675, Dec. 2008.

[20] B. J. Chun and M. P. Kennedy, "Statistical properties of first-order bang-bang PLL with nonzero loop delay," *IEEE Trans. Circuits Syst. II, Exp Briefs.*, vol. 55, no. 10, pp. 1016–1020, Oct. 2008.

[21] R. Kreienkamp, U. Langmann, C. Zimmermann, T. Aoyama, and H. Siedhoff, "A 10-gb/s CMOS clock and data recovery circuit with an analog phase interpolator," *IEEE J. Solid-State Circuits*, vol. 40, no. 3, pp. 736–743, Mar. 2005.

[22] A. J. Hayter, *Probability and Statistics for Engineers and Scientists*, 2nd ed. Pacific Grove, CA: Duxbury Press, 2001.

Joon-Yeong Lee was born in Seoul, Korea. He received the B.S. degree in electrical engineering from Korea Advanced Institute of Science and Technology (KAIST), Daejeon, Korea, in 2011, where he is currently working toward the M.S. degree.

His research interests include PLL, CDR, and high-speed serial links for optical fibers.

Hyeon-Min Bae received the B.S. degree in electrical engineering from Seoul National University, Seoul, Korea, in 1998 and the M.S. and Ph.D. degrees in electrical and computer engineering from the University of Illinois at Urbana-Champaign in 2001 and 2004, respectively.

In 1996, he served his military duty. From 2001 to 2007, he lead the analog and mixed-signal design aspects of OC-192 MLSE based EDC ICs at Intersymbol Communications, Inc., Champaign, IL. From 2007–2009, he was with Finisar Corporation (NASDAQ: FNSR) after its acquisition of Intersymbol Communications Inc. Since 2009, he has been an Assistant Professor of electrical engineering in Korea Advanced Institute of Science and Technology (KAIST), Daejeon, Korea, where his research has been focused on high-speed clock-data recovery systems.

Dr. Bae received the 2006 IEEE JOURNAL OF SOLID-STATE CIRCUITS Best Paper Award.